

PAPER • OPEN ACCESS

Table-top laser-based proton acceleration in nanostructured targets

To cite this article: M Blanco *et al* 2017 *New J. Phys.* **19** 033004

View the [article online](#) for updates and enhancements.

Related content

- [Review of laser-driven ion sources and their applications](#)
Hiroyuki Daido, Mamiko Nishiuchi and Alexander S Pirozhkov
- [Short pulse laser interaction with micro-structured targets: simulations of laser absorption and ion acceleration](#)
O Klimo, J Psikal, J Limpouch *et al.*
- [Enhanced ion acceleration in transition from opaque to transparent plasmas](#)
R Mishra, F Fiuza and S Glenzer

Recent citations

- [Enhancement of laser-driven ion acceleration in non-periodic nanostructured targets](#)
J. Ferri *et al*
- [Generation of ultra-energetic ions by interaction of petawatt lasers with micrometer-scale foils](#)
A. Héron *et al*
- [Target normal sheath ion acceleration by fs laser irradiating metal/reduced graphene oxide targets](#)
L. Torrisi *et al*



PAPER

Table-top laser-based proton acceleration in nanostructured targets

OPEN ACCESS

RECEIVED

30 November 2016

REVISED

19 January 2017

ACCEPTED FOR PUBLICATION

9 February 2017

PUBLISHED

1 March 2017

Original content from this work may be used under the terms of the [Creative Commons Attribution 3.0 licence](https://creativecommons.org/licenses/by/4.0/).

Any further distribution of this work must maintain attribution to the author(s) and the title of the work, journal citation and DOI.

M Blanco¹, M T Flores-Arias¹, C Ruiz² and M Vranic³

¹ Photonics4Life Research Group, Departamento de Física Aplicada, Facultad de Física, Universidade de Santiago de Compostela, Campus Vida s/n, 15782 Santiago de Compostela, Spain

² Instituto Universitario de Física Fundamental y Matemáticas and Departamento de Didáctica de la Matemática y de las Ciencias Experimentales, Universidad de Salamanca, Patio de las Escuelas s/n, Salamanca, Spain

³ GoLP/Instituto de Plasmas e Fusão Nuclear, Instituto Superior Técnico, Universidade de Lisboa, 1049-001 Lisbon, Portugal

E-mail: manuel.blanco.fraga@usc.es and maite.flores@usc.es**Keywords:** laser-plasma interaction, particle in cell simulations, laser-driven acceleration, nanostructured targets, laser ion acceleration, TNSA

Abstract

The interaction of ultrashort, high intensity laser pulses with thin foil targets leads to ion acceleration on the target rear surface. To make this ion source useful for applications, it is important to optimize the transfer of energy from the laser into the accelerated ions. One of the most promising ways to achieve this consists in engineering the target front by introducing periodic nanostructures. In this paper, the effect of these structures on ion acceleration is studied analytically and with multi-dimensional particle-in-cell simulations. We assessed the role of the structure shape, size, and the angle of laser incidence for obtaining the efficient energy transfer. Local control of electron trajectories is exploited to maximize the energy delivered into the target. Based on our numerical simulations, we propose a precise range of parameters for fabrication of nanostructured targets, which can increase the energy of the accelerated ions without requiring a higher laser intensity.

1. Introduction

Ion acceleration in laser-driven plasma accelerators has been a very active field in the last few years. It has been demonstrated that it is possible to accelerate ions up to energies of tens of MeV with table top laser sources [1–3]. One of the most robust mechanisms used to accelerate ions in plasma based accelerators is the target normal sheath acceleration (TNSA). In this mechanism a high intensity laser interacts with a few-micron thick solid target to produce energetic ions [4–7]. The laser pulse ionizes the target surface and heats up the electrons; these electrons propagate across the target and escape perpendicularly to the rear surface. This generates a space charge separation in the rear surface that yields a strong longitudinal field which can accelerate positively charged particles located in the vicinity of the surface.

Solid targets for plasma-based accelerators can be manufactured with a variety of properties to make the acceleration more efficient. This subject has received a wide attention because the optimization of the targets opens a way to produce more energetic ions without the need of increasing the laser power. Different approaches such as varying the target thickness [8], nanostructuring the back surface of the target [9, 10] or growing a layer of low density foam [11–13] have already been studied. Several publications have reported that adding periodic nanostructures on the target front surface enhances drastically the laser energy absorption [13–21]. This generates ions with much higher energies than the ones obtained when targets with a flat surface are used [13, 20–30]. The nature of this enhancement is still a matter of discussion, however it is known that it is strongly dependent on the shape of the structures, as well as on the angle of incidence of the impinging laser [13–15, 17, 18, 21, 22, 26, 27].

As there are several laser absorption mechanisms in overdense plasmas, such as the generation of surface plasma waves (SPW) [13, 15, 16, 29, 31–35], resonant absorption, vacuum heating or $J \times B$ heating [36–38], one can use nanostructures with properties especially suited to enhance a particular absorption mechanism. Our aim

is to optimize the acceleration of electrons in the vacuum gaps of a periodic structure, so-called vacuum heating [17, 21, 27].

The main purpose of this work is to show how the geometry of periodic structures can be optimized to achieve a higher laser energy absorption and proton energies, in particular for the specification of the STELA laser of the L2A2 facility of the University of Santiago de Compostela, with laser intensities on the order of $10^{19} \text{ W cm}^{-2}$ and a peak power on the order of tens of TW. We present an analytical and numerical study of the interaction of laser pulses and solid targets with triangular periodic nanostructured surfaces. The dimensions of the structures dictate the time electrons spend interacting with the laser field in the free spaces within the structure which directly influences the ratio of laser energy absorbed by the electrons. The reason behind the observed enhanced absorption and higher proton energies is the possibility to control the recollision time of the electrons by changing the parameters of the triangular structure.

We propose an optimal structured surface for energy absorption and energetic proton production that can be fabricated and used experimentally, providing a robust strategy to obtain higher energy protons without the need of using a higher laser intensity. We introduce a simple analytical model for the laser energy absorption by the plasma electrons as a function of the nanostructure dimensions. The predictions of this model are in good agreement with our particle-in-cell (PIC) simulation results. In addition, we study the effects of using oblique laser incidence, and propose an alternative structured target surface optimized for oblique incidence.

This paper is structured as follows: section 2 introduces an analytical model to account for the increase in the energy absorption due to the presence of the periodic nanostructures. Section 3 contains 2D PIC simulations, where a wide range of parameters was studied to find the optimal target design for maximal laser absorption and proton cutoff energy. Section 4 accounts for differences between 2D and 3D geometry. The effect of using oblique incident laser pulses is addressed in section 5, in which we propose an optimal experimental configuration to obtain energetic protons. The summary and discussion of our results are presented in sections 6 and 7.

2. Analytical model of electron dynamics

In this section we introduce a simple analytical model to understand the electron motion in the presence of the laser field within the periodic structures. The laser energy absorption is directly related to the electron heating, as electrons are the lightest particles in the plasma and the first to interact with the laser field. Understanding how electrons absorb the laser energy and carry it towards the rear of the target is crucial to select an optimal surface structure.

The use of triangular structures in the front face of the target changes the local angle of incidence of the laser and allows electrons to undergo a temporary interaction with the laser field in vacuum before recolliding with the target. As the laser arrives to the target, it strips off a portion of the electrons from the lateral surface of the structure. The electrons are accelerated by the laser field in the vacuum gaps of the structures and gain energy. They reenter the target where the laser cannot penetrate and deliver their energy into the target, as shown in figure 1. The shape of the triangular structures determines the time the electrons spend being accelerated in the vacuum gap and their recollision energy. We expect an optimal laser absorption for targets with geometrical properties that allow for maximum electron energy gain.

A simple model that neglects all fields except the laser is useful to understand how the recollision energy is related to the triangle shape. Our starting point is to consider the relativistic motion of an electron in vacuum under the influence of a linearly polarized electromagnetic wave given by the vector potential

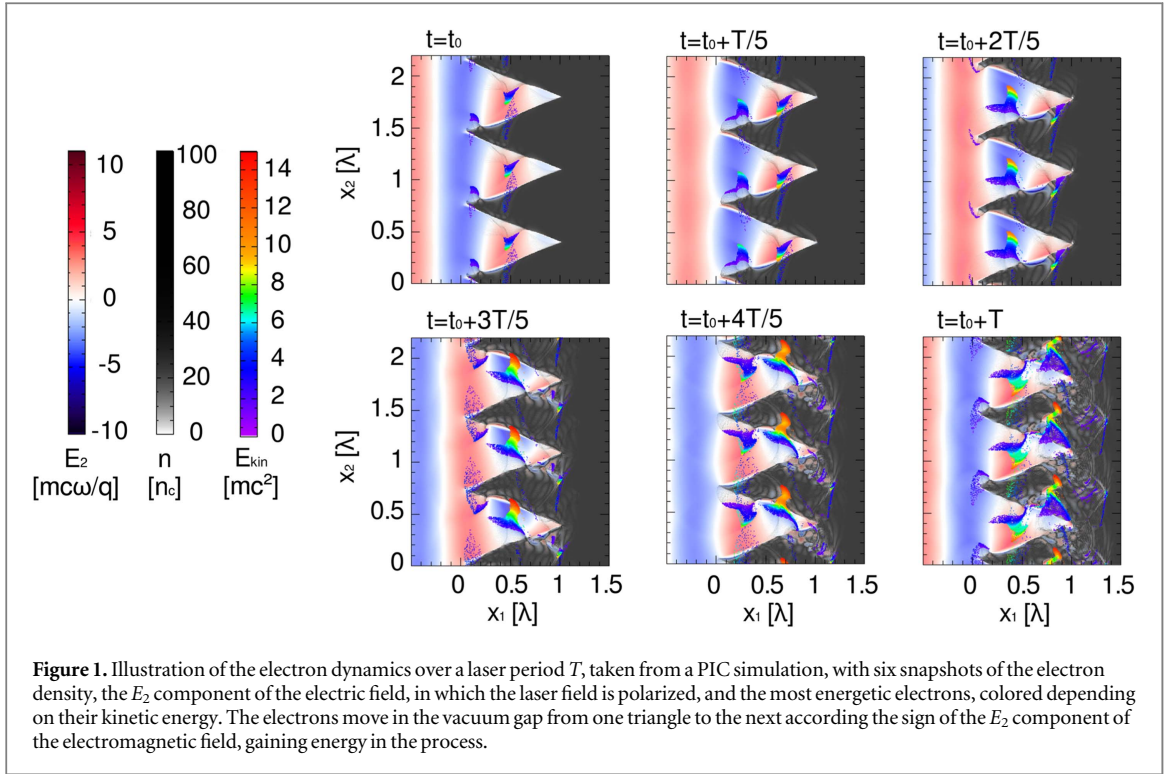
$$\vec{A} = a_0 \frac{m_e c}{\omega} \sin(\varphi) \hat{x}_2, \text{ where } a_0 \text{ is the dimensionless vector potential defined by } a_0 = 0.85 \left(\frac{I \lambda^2}{10^{18} \text{ W cm}^{-2} \mu\text{m}^2} \right)^{\frac{1}{2}},$$

where I is the laser intensity in W cm^{-2} and λ the laser wavelength in μm . The variable $\varphi = \omega t - \vec{k} \cdot \vec{r} + \varphi_0$ represents the electromagnetic wave phase, \vec{k} is the wave vector, \vec{r} the particle position, ω the angular frequency, t the time and φ_0 is the initial phase. The equation of motion of an electron in the vacuum gap is determined by the Lorentz force:

$$\frac{d\vec{p}}{dt} = -q_e \vec{E} - q_e \left(\frac{\vec{p}}{\gamma m c} \times \vec{B} \right) = \frac{q_e}{c} \frac{\partial \vec{A}}{\partial t} - q_e \left(\frac{\vec{p}}{\gamma m c} \times (\vec{\nabla} \times \vec{A}) \right), \quad (1)$$

where q_e is the electron charge. This equation can be solved for the specified vector potential assuming that the electron is initially at rest and that for $t = 0$ we have $\varphi = 0$. The momentum and displacement of the electron are then given by [36]:

$$p_1 = \frac{a_0^2}{2} m_e c \sin^2(\varphi) \quad p_2 = a_0 m_e c \sin(\varphi), \quad (2)$$



$$\Delta x_1 = \frac{a_0^2}{8\pi} \lambda \left(\varphi - \frac{\sin(2\varphi)}{2} \right) \quad \Delta x_2 = \frac{a_0}{\pi} \lambda \sin^2 \left(\frac{\varphi}{2} \right), \quad (3)$$

where the indexes '1' and '2' refer to the longitudinal and transverse field directions and $\lambda = 2\pi c/\omega$ is the laser field wavelength.

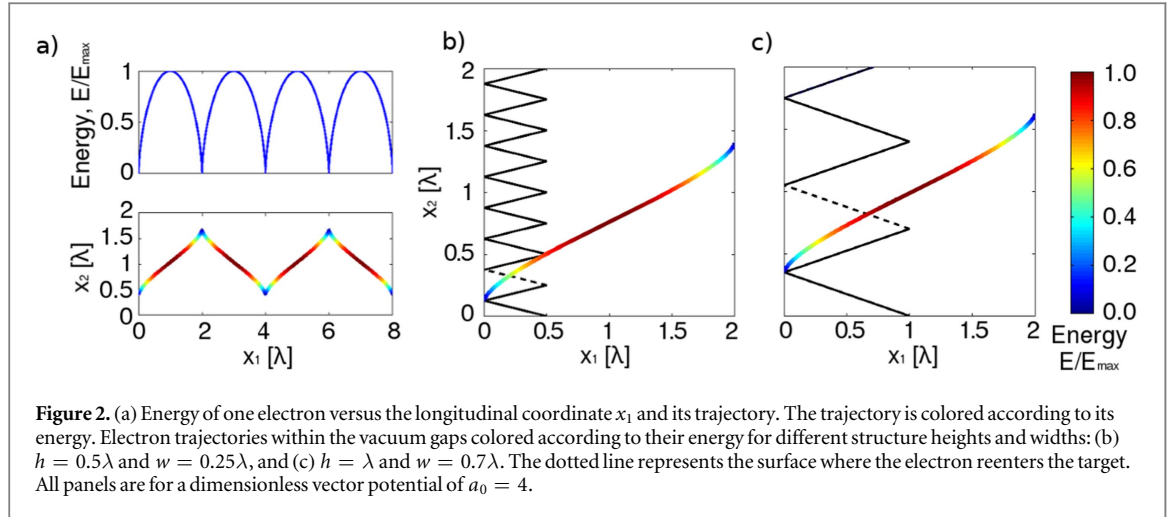
The maximum electron energy is reached when $\varphi = \pi/2$, because both components of the electron momentum are maximized, so if the electrons reenter the target at this point they will absorb the maximum possible energy from the field. Reaching the optimal phase at the moment when the electron reenters the target is controlled by its initial position in the structured surface, expressed by its initial height, h_0 . We can establish a relation between the initial height where a single electron is located and the phase when it arrives to the surface of the next triangle by using the displacements in equation (3). This relation is obtained from the following relation for the triangle angle:

$$\tan(\alpha) = \frac{h}{w/2} = \frac{x_{1f}}{x_{2f}} = -\frac{h_0}{x_{2o}}, \quad (4)$$

where h and w are the structure height and width and the indexes 'o' and 'f' indicate original and final position at the periodic structure surface, respectively. Taking into account the definition of the displacements $\Delta x \equiv |x_f - x_o|$, we can obtain the final equation $h_0 = \Delta x_1 \frac{1}{2} + \Delta x_2 \frac{h}{w}$, which, written in our variables of interest, is:

$$h_0(\varphi) = \frac{a_0^2}{16\pi} \lambda \left(\varphi - \frac{\sin(2\varphi)}{2} \right) + \frac{a_0}{\pi} \frac{h}{w} \lambda \sin^2 \left(\frac{\varphi}{2} \right). \quad (5)$$

The maximum amount of energy absorbed by the electrons in the gap is reached when $h_0(\varphi = \pi/2) \approx h$, because this means that the electrons initially located at the tip of the structure gain the maximum possible energy. These electrons are the first to interact with the laser pulse. If $h_0(\varphi = \pi/2) > h$ the electrons will not reach the maximum energy because their ideal initial height is not allowed on the structure and when $h_0(\varphi = \pi/2) < h$ a portion of the electrons at the top of the structure will stay longer in the vacuum gaps and not enter the target with the optimal energy. It can be also noted that the second term on the right hand side of equation (5) becomes less relevant as a_0 increases. However, the findings of equation (5) cannot be applied directly to very high intensities where the hole-boring can destroy the pre-formed structures before the end of the interaction. We therefore restrict our analysis to a moderate laser intensity. Using a laser field with a dimensionless amplitude of $a_0 = 4$, which can be achieved with the laser STELA, the equation (5) for the maximum electron energy becomes:



$$h_0(\varphi = \pi/2) = \frac{\lambda}{2} + \frac{2}{\pi} \frac{\lambda}{w} h. \quad (6)$$

The value of h_0 relative to h in the previous equation is controlled by the width of the structures. For $w \ll 2\lambda/\pi$ then $h_0 \gg h$ and viceversa. Therefore, there is an optimal structure width for improving the energy absorption, given by $w = 0.64\lambda$. When the structure width has this value, equation (6) becomes $h_0(\varphi = \pi/2) = \lambda/2 + h$, which means that for higher structures ($h \gg \lambda/2$) we get $h_0 \rightarrow h$. We therefore expect that above a certain structure height ($h \sim 0.5\lambda$) the energy absorption percentage reaches a maximum value and does not change further. This simple model provides a clear picture on how the engineering of the triangular structures can be used to control the electron trajectories and maximize the energy they deliver to the target.

Figure 2 depicts the energy and motion of an electron under equations (2) and (3) and shows that the structure shape can be manipulated to obtain maximum absorption from the electrons moving from the tip of one triangle across the vacuum gap. Figure 2(a) shows that there is a maximum energy, reached periodically for certain positions that would correspond to the phase $\varphi = (2N + 1)\pi/2$, where N is an integer. Figures 2(b) and (c) show, for different structure heights and widths, the trajectory of an electron moving in the vacuum gap, colored according to its energy. It can be observed that the shape of the structure influences the energy that the electron has at the recollision time; the energy is lower in figure 2(b) than in 2(c).

The predictions obtained from the model for the dependence of the energy absorption with the structure height and width can be tested by performing PIC simulations. In the following sections we discuss the results obtained from such simulations, with the aim of designing an optimal target for energy absorption and ion acceleration.

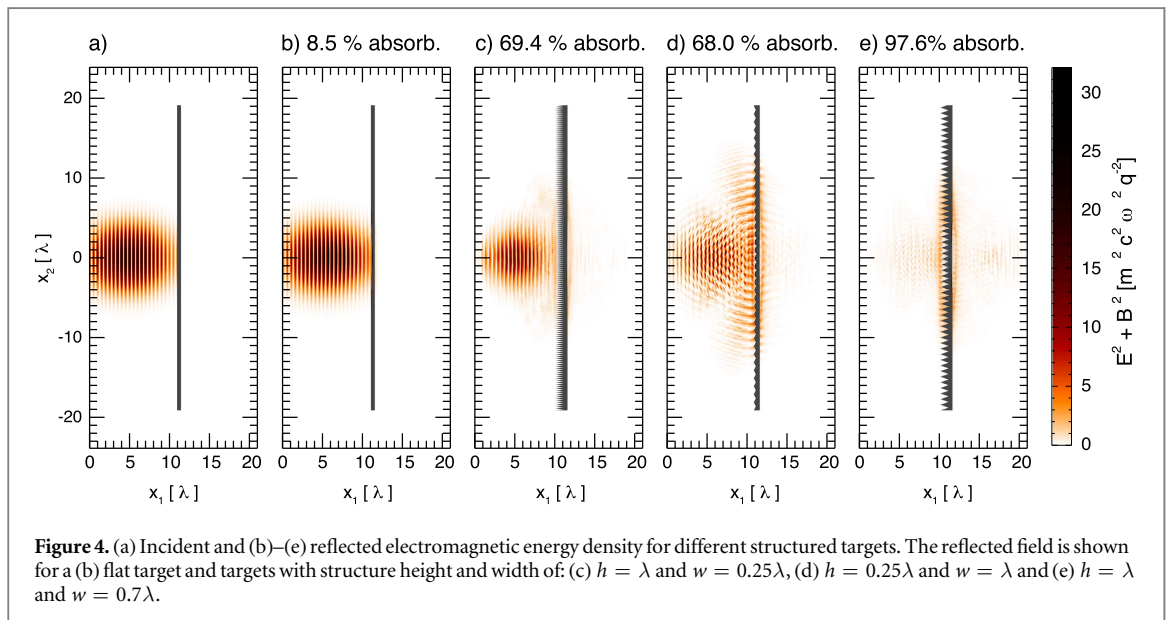
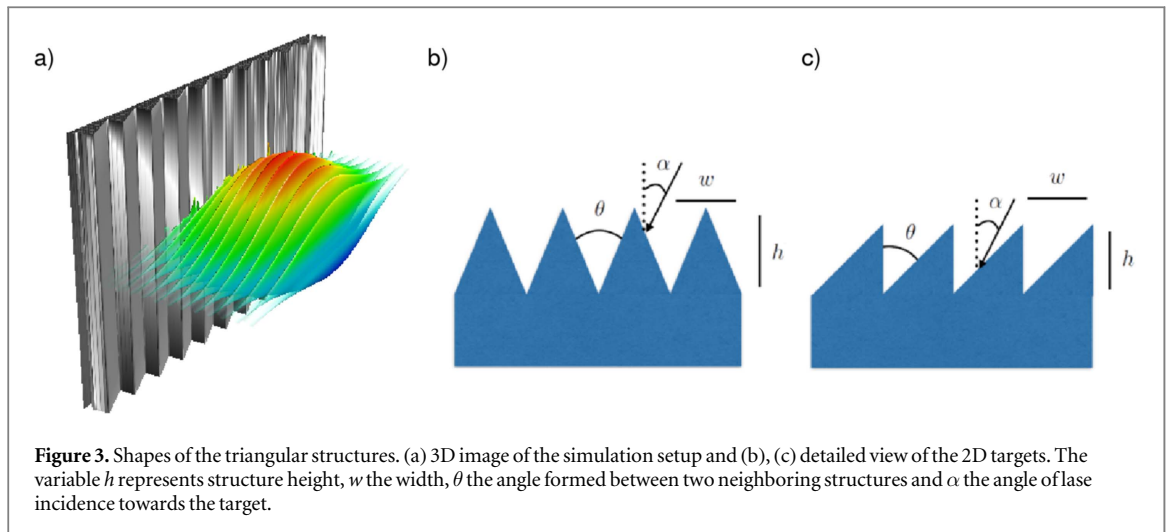
3. Effect of the structure shape and size on the laser energy absorption and proton acceleration

The aim of this section is to identify a parameter range with maximum transfer of laser energy to the accelerated protons. To address how the shape of the structures affects the absorption of laser energy as well as the energies of the electrons and protons, we present a numerical study encompassing a wide range of sizes for two types of structures indicated in figure 3. We vary their width and height and use a laser pulse at normal incidence.

Numerical simulations of the laser-plasma interaction are performed with the PIC code OSIRIS [39]. In OSIRIS, the fields are stored on a discretized spatial grid and advanced according to the Maxwell's equations. The particle motion is determined by the relativistic Lorentz force.

Two different targets with triangular structures were used in this work, as shown in figure 3. The reasons behind choosing these structures are that they yield high absorption rates and efficient proton acceleration in comparison with other kinds of structures [18, 22] and can be manufactured for their use in experiments. The asymmetry presented in figure 3(c) ('tilted triangles') with respect to figure 3(b) ('regular triangles') is interesting from the experimental point of view, where oblique incident laser pulses are going to be used.

The targets are made of electrons and protons with a number density of $n = 40n_c$, where $n_c = \frac{m_e \omega^2}{4\pi q_e^2}$ is the critical plasma density. All the targets have a bulk thickness of 0.5λ (unless specified differently), where λ is the wavelength of the laser, and the number of particles per cell is 16 per species. The density has a steep profile as we



consider a high contrast laser ($> 10^{10}$ at 5 ps) which corresponds to the STELA laser. The simulation box has a width and length of $38.3 \mu\text{m}$ and $16.9 \mu\text{m}$, respectively. The spatial resolution is $\delta = 2.55 \text{ nm}$ in both axes.

The laser pulse is focused on the target surface. This pulse is launched from the left wall of the simulation box, located at a distance of $8.9 \mu\text{m}$ to the target. The laser has an intensity of $3.45 \times 10^{19} \text{ W cm}^{-2}$, a FWHM of 25 fs (with a \sin^2 temporal profile), a wavelength of $\lambda = 800 \text{ nm}$ and a spot diameter of $6 \mu\text{m}$. The laser pulse is linearly polarized in the simulation plane, such that it is always p-polarized in relation to the structures.

The simulation advances in timesteps of 4.26 as. The reflected energy, as well as the electron properties at the rear surface, are measured right after the interaction finishes, at the time 70.2 fs. The proton properties are measured at 172.3 fs, the time at which electrons that generate the accelerating field start leaving the simulation box. The reflected energy is measured by integrating the reflected field energy density. We have also monitored the electron and proton kinetic energy, as well as the energy of the self-consistent fields generated around the target. The energy conservation has been verified throughout all the simulations. The electron temperature at the rear surface is obtained by fitting the electron spectrum to a Maxwell–Jüttner distribution. The simulation setup is designed to scan the parameter space and compare the relative gain between the flat and structured targets.

Several cases from low to almost complete laser absorption are illustrated in figure 4, figure 4(a) shows the incident laser pulse and figures 4(b)–(e) display the reflected fields. The lowest absorption is obtained for a flat target. The results obtained for different structured targets are displayed in figures 4(c)–(e). We observe that the reflected spatial distribution of light when structured targets are used carries the imprint of the nanostructures at the target surface, and more laser energy is absorbed.

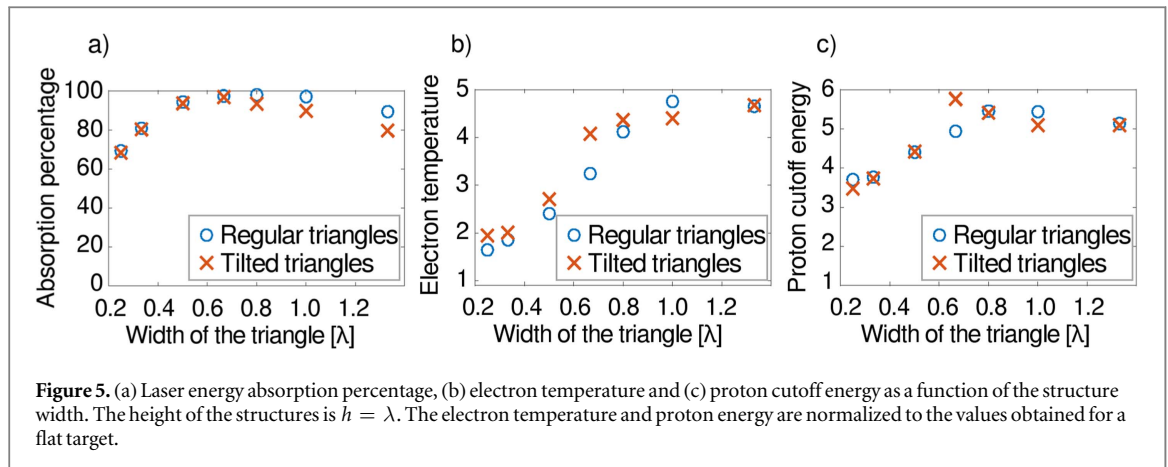


Figure 5. (a) Laser energy absorption percentage, (b) electron temperature and (c) proton cutoff energy as a function of the structure width. The height of the structures is $h = \lambda$. The electron temperature and proton energy are normalized to the values obtained for a flat target.

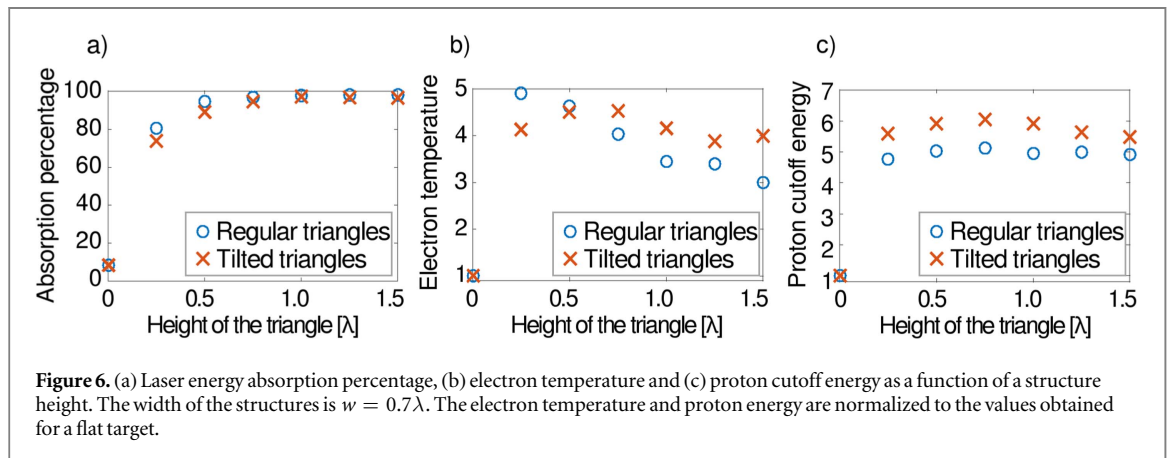


Figure 6. (a) Laser energy absorption percentage, (b) electron temperature and (c) proton cutoff energy as a function of a structure height. The width of the structures is $w = 0.7\lambda$. The electron temperature and proton energy are normalized to the values obtained for a flat target.

To verify the predictions of section 2, we perform a first set of simulations with a fixed structure height of $h = \lambda$, where we vary the structure width. According to our analysis we should expect maximum energy absorption at a width of $w \sim 0.64\lambda$. Figure 5(a) shows the energy absorption, as a function of the structure width, for regular and tilted triangular nanostructures. In both cases the energy absorption increases with the width of the triangles up to a maximum nanostructure width around 0.7λ . Above this value the energy absorption decreases smoothly as the triangle width increases. For the triangles 0.6λ – λ wide, we obtain that the energy absorption is above 90%. The increase in electron temperature is shown in figure 5(b): it rises with the width of the triangles for both types of structures. Once the width of the triangles becomes close to 0.7λ the slope of the curve changes to a lower value. The gain in proton cutoff energy is shown in 5(c). It exhibits a similar trend as the energy absorption.

The plots in figure 5 show that the structure width can be optimized to yield a maximum laser absorption and proton energy cutoff. The structure width of the optimal target is consistent with the analytically predicted $w = 0.64\lambda$.

A second set of simulations is performed with a fixed structure width of $w = 0.7\lambda$ and varying the structure height. We kept the rest of simulation parameters equal to the ones in the previous case. Here we should expect nearly a complete laser energy absorption above a certain threshold structure height. Figure 6 displays the energy absorption, the relative electron temperature and proton cutoff energy versus the height of the structures. The energy absorption percentage is shown in figure 6(a), that depicts an increase of the absorption of energy as the height of the triangles becomes bigger, up to a maximum value, close to 100%. Once this maximum is achieved, it remains unchanged as we increase the height of the triangles. The electron temperature, in figure 6(b), shows a big increase when the structures are added, followed by a smooth decay/stabilization for higher structures. Figure 6(c) displays the relative proton cutoff energy.

For $h > 0.5\lambda$, the results in figure 6 show that the absorption percentage is above 90% and there is a five-fold increase in the proton cutoff energy compared with the flat target. The high absorption percentages shown in figure 6(a) are due to the choice of a structure width of 0.7λ , close to the optimal value found before. As predicted by the analytical model, above the threshold structure height, the laser energy absorption is nearly 100% and there is no significant difference observed in the spectrum of generated protons.

Figures 5 and 6 demonstrate that there is a correspondence between the trend followed by the laser absorption and the cutoff energy of the protons. This is not surprising, because in TNSA the absorbed laser energy is carried by the electrons towards the rear side of the target. These electrons escape the target and create a longitudinal field proportional to the square root of the electron temperature and to the electron front number density [6]. This longitudinal field is responsible for the acceleration of protons. We therefore expect higher proton energies for higher achieved electron temperatures at the rear surface. However, additional height in the structures changes the effective target thickness and hence the electron front number density is also modified. The consequence is that the electrons with a lower temperature (e. g. for $h = 1.5\lambda$ in figure 6(b)) can, in principle, generate the accelerating field of the same magnitude as the electrons with a 53% higher temperature in a case with a different effective target thickness (e. g. for $h = 0.5\lambda$ in figure 6(b)). We therefore obtain similar values for the accelerating field and for the proton cutoff energy in all cases where $h > 0.5\lambda$.

4. Comparison between 2D and 3D results

We have analyzed how the energy absorption varies when triangular structures are on the target surface and how this variation affects the electron heating and consequently the energies of the accelerated protons. Our theoretical analysis, combined with 2D PIC simulations, shows that the structure shape can be optimized to yield high percentages of energy absorption, which is in agreement with previous publications [17, 21, 27].

The values obtained for the optimal height and width in terms of energy absorption are given by a width of $w = 512$ nm and a lower bound for the structure height of $h \sim 400$ nm. Fabrication of these structures is achievable by current techniques, therefore the targets described here can be manufactured in a cost effective way and used experimentally [13, 18, 22, 23].

Our conclusions regarding the target structure for optimal laser absorption are general and can be extended to 3D geometry. The electron interaction with an electromagnetic wave in vacuum is fully described in 2D. The energy of the electrons at the point of re-entry into the target depends on the geometrical properties of the structures such as width and height and it is intrinsically a 2D problem. The optimal configuration for laser absorption is therefore likely to be the same in 2D and 3D geometry. However, even though ion acceleration can be studied qualitatively in 2D, it is well-known that the proton energy cutoff in TNSA is lower in 3D geometry [40, 41].

Due to limited computational resources, it is not possible to perform a full-scale 3D simulation and allow enough time for target expansion. However, the 3D simulations can be performed in slab geometry. In this geometry the laser is treated as a wavepacket that is transversely a plane wave and periodic transverse boundary conditions are applied both for the fields and the particles, except for the direction of laser propagation where open boundaries are used.

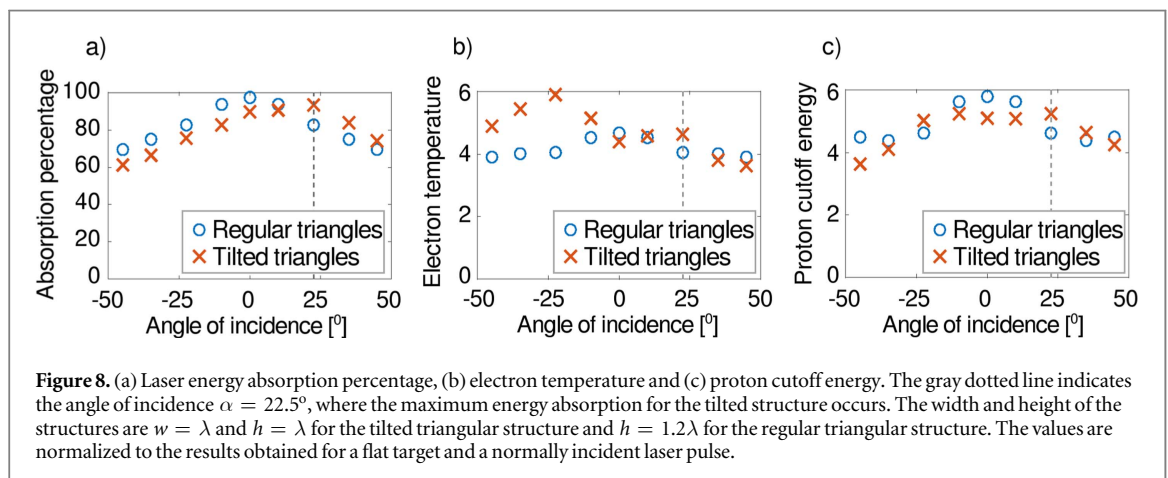
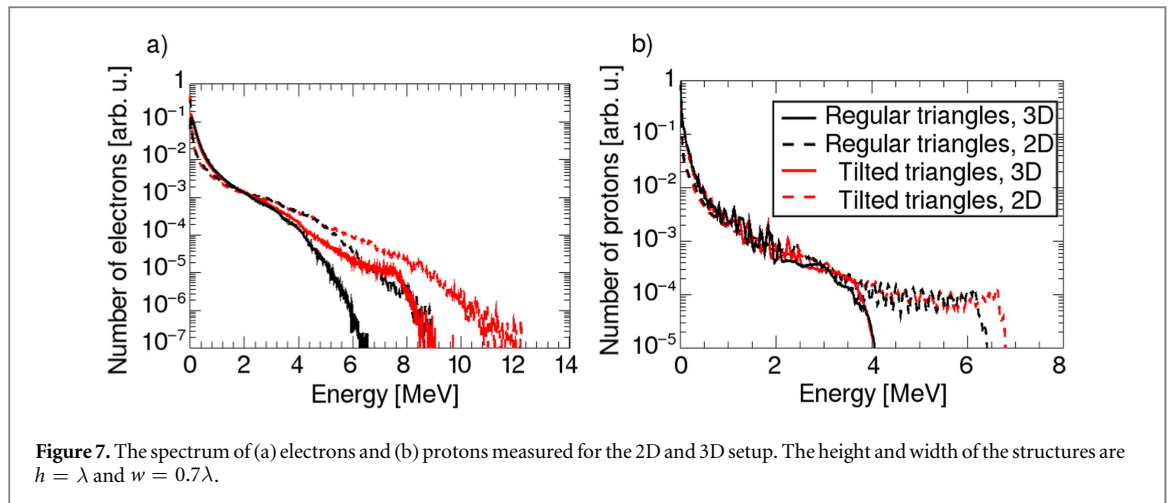
The simulation box is 25λ long and $3.5\lambda \times 3.5\lambda$ wide. The laser pulse is initialized inside the box with a total duration of $7T$, where $T = c/\lambda$ is the laser period, and a distance of 0.5λ to the structure tip. We performed simulations for optimal structured targets where $h = \lambda$ and $w = 0.7\lambda$ and for flat targets, with a goal to compare the relative increase of the absorption efficiency in 2D and 3D.

In 3D simulations we obtained 91.5% of laser absorption for regular, 89.5% for tilted triangles and 2% for a flat target. In 2D simulations, the 95.4% was absorbed for regular, 92.3% for tilted triangles, and 2.6% for the flat target. The absorption estimates from 2D and 3D are consistent within a margin of 4%. There is approximately a 15-fold increase in the proton cutoff energy when we use structured targets instead of flat ones in 3D.

The electron spectra from 2D and 3D simulations at the time 25.5 fs are displayed in figure 7(a). They are normalized to the same reference height at the energy 2 MeV. We can observe a slight difference between the tilted and regular structures, due to different electron dynamics at the target surface. The respective proton spectra at the time 51.1 fs are shown in figure 7(b). These spectra are normalized to the same reference height at the energy 1 MeV. As expected, the proton cutoff is lower in 3D compared to the 2D case. Apart from verifying the conclusions obtained in 2D, an additional advantage of 3D simulations is that they can provide an estimate of the total number of accelerated protons. In our case the number of protons being accelerated to an energy above 0.1 MeV is approximately 1.35×10^{11} , corresponding to over ~ 21.6 nC of charge accelerated to energies up to 4 MeV. As the transverse box dimensions are chosen to be on the order of the laser spotsize, this is the approximate number of protons per shot expected in an experiment with similar conditions.

5. Oblique laser incidence

In the previous sections it has been discussed how the energy absorption and the particle properties change with the front structure shape of the solid target. All the previous simulations have been performed with a pulse in normal incidence, however experiments of TNSA proton acceleration are typically done in oblique incidence.



The main reason for using oblique incidence is to avoid the damage on the optical elements used to transport the beam to the target, with the particles ejected by the target or the back reflection of the laser pulse.

The angle of incidence of the laser pulse is expected to affect the laser energy absorption and the particle energies. We have performed simulations at different angles of incidence using targets with $w = \lambda$ and $h = 1.2\lambda$, for regular and $w = \lambda$ and $h = \lambda$ for tilted triangles.

Figure 8 displays (a) the energy absorption, (b) the electron temperature and (c) the proton cutoff energy at oblique laser incidence. Figure 8(a) shows that for the regular triangular structure, the maximum absorption and particle energies occur at normal incidence, while for the tilted structures this maximum is shifted by a value close to 22.5° . The electron temperature for the tilted structures, in 8(b), displays two maxima at the angles $\pm 22.5^\circ$, while the proton cutoff energy for the same structure, in 8(c), shows a plateau around the zero angle slightly maximized for the maximum energy absorption angle.

The peak observed for the electron temperature at $\alpha = -22.5^\circ$ represents electrons that get heated efficiently but do not contribute to enhance the energy of TNSA protons. This behavior suggests that a SPW [16, 29, 31–35] is being excited at this angle, such that the electrons escape the target tangentially. This is confirmed by measuring the longitudinal accelerating field in the rear surface of the target, which shows the same trend as the proton cutoff energy in figure 8(c).

The analysis of the effect of oblique incident pulses shows that the asymmetric tilted triangles yield to a higher absorption percentage and more energetic protons at oblique incidence compared to normal incidence. We have performed an additional simulation combining an oblique incident laser pulse with an optimized height and width of the structure $h = \lambda$ and $w = 0.7\lambda$. The bulk target thickness is 2λ and the angle of incidence of the laser is $\alpha = 17.5^\circ$.

The comparison between the results obtained with the same setup for a target with a flat surface and the structured target show a 15-fold increase in the energy absorption percentage, from a 6.1% in the flat target to a 90.6% in the structured target. This enhancement of the energy absorption generates protons with energies between 4 and 5 times higher compared with the case in which a flat solid target was used. This is verified in figure 9 that shows (a) the proton energy spectrum and the momentum space p_1 - p_2 of the protons. Both, the

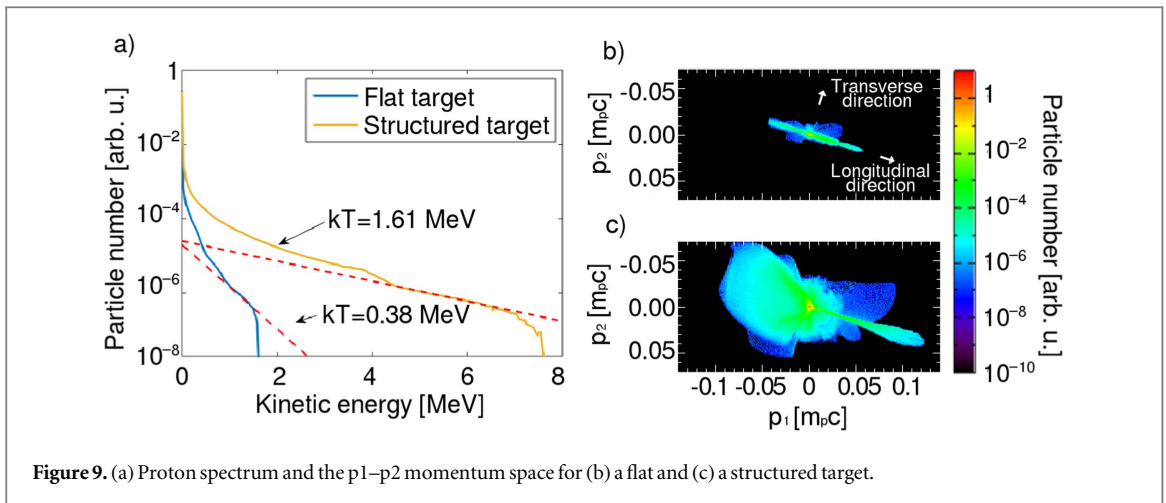


Figure 9. (a) Proton spectrum and the p_1 – p_2 momentum space for (b) a flat and (c) a structured target.

cutoff energy and the temperature of the protons increase by a factor between 4 and 5 when one uses a structured target in place of a flat one.

The result shown in figure 9 demonstrates in an experimentally feasible setup that the use of surface nanostructured targets can increase substantially the energy of the accelerated protons.

6. Discussion on other target features

We have studied various parameters that affect how periodic triangular structures on solid targets can enhance the energy absorption from a laser to a solid target. However, there are several factors relevant to the ion acceleration we have not addressed. This section discusses how our conclusions can be affected by using a different nanostructure shape, or by varying the target thickness and compounds, or adding preplasma.

The enhanced energy absorption can be obtained also with other structure geometries, such as rectangles [17, 21, 27] or nanospheres [20, 22]. Our model can, in principle, be extended to account for different structure geometries. As the key parameter for obtaining an optimal laser absorption is the time-of-flight of the electrons in the vacuum gap, a change in the shape of the structure directly affects their energy at the point of recollision with the target. Also, certain shapes that are not grating like might add different dynamics at the target surface. We therefore expect that other structures would have different absorption percentages.

In studies using nanospheres, it has been reported that a very short preplasma of length 0.04λ changed the absorption percentage by 5% [22]. In [17, 21, 27], the effect of preplasma on nanostructured targets is also discussed and they conclude that a low contrast and hence a long preplasma region would destroy the structures before the main pulse arrives. In our simulations we have considered that the plasma has a steep profile. This is justified by the specifications of the laser system considered, that presents a high contrast ($> 10^{10}$ at 5 ps). Nonetheless, a small plasma expansion can be expected before the main pulse arrives to the target surface. Based on our analytical model, the existence of a pre-plasma with short scale length ($\ll \lambda$) could be slightly detrimental to the enhanced absorption, since the time-of-flight of the electrons within the vacuum gaps is going to be different.

We have performed additional simulations to verify the effect that a short preplasma region has on the laser absorption for the specifications of our system. These simulations have been performed in slab geometry, using a simulation box 21λ long and 7λ wide, and keeping the rest of the parameters equal as in the simulations above. For the targets with an optimal design ($h = \lambda$ and $w = 0.7\lambda$), the variations due to the plasma pre-expansion are found to be very small. The target without any preplasma absorbs 96.5% of the laser energy. If one considers a preplasma length of 0.5λ , the absorption decreases to 90.1%, while for a smaller preplasma of 0.1λ the target absorbs 96.0% of the energy. In the latter case, the energy absorption is reduced by less than 1%.

The target thickness is another relevant parameter for proton acceleration [8]. Although the aim of this paper is to address the effect of the triangular nanostructures, we have studied briefly the outcome of varying the target thickness from 0.25λ to 2λ . The laser energy absorption did not change. However, the thickness of the target affects the proton acceleration, since it determines the redistribution of energy from the electrons to the protons. As the laser absorption is not affected by this, our optimal structures can be added to the front surface of a target of an arbitrary thickness, and ensure that the maximum possible energy is transferred from the laser to the electrons. In other words, the target structure shape and the target thickness can be optimized separately to result in the most efficient proton acceleration.

A similar conclusion can be made for the effect of using compound targets on proton acceleration. In this manuscript, we present simulations of hydrogen targets, but most TNSA targets in experiments are composed of heavy ions and electrons with a thin proton contamination layer on the rear surface [1, 2, 4, 7]. The presence of different compounds is expected to change the energy of the accelerated protons. However, the dynamics of the electrons near the front surface will be similar as in our hydrogen simulations, because their motion depends on the geometry of the nanostructures. We verified that neither a higher ion mass nor a higher plasma density significantly affect the laser absorption, by performing a set of simulations with targets made of fully ionized silicon with plasma density of $400n_c$. The optimal structure for energy absorption and the absorbed energy remains unchanged.

The best strategy for target fabrication is to combine several different aspects of optimization in order to obtain the highest ion energies (or higher yield of ions at lower energies). Using nanostructures at the front surface presents an opportunity for an additional increase in efficiency of the laser energy absorption by the electrons, which is compatible with other types of target optimization.

7. Conclusions

The acceleration of protons in laser plasma accelerators using thin targets with periodic nanostructures has been studied. We have performed 2D and 3D PIC simulations to reveal how the energy absorption and the accelerated proton kinetic energies vary with the shape of the structures and the angle of incidence of the laser.

The use of triangular periodic structures at the target front surface increases the laser energy absorption and the proton kinetic energy. Through an analytical and numerical study, we have found that these quantities can be maximized by tailoring the dimensions of the nanostructures.

Through the right choice of the dimensions of the structures and the angle of incidence of the laser, energy absorption percentages on the order of 90% can be achieved, yielding to an increase on the proton kinetic energy between 4 and 5 times in comparison to those that can be achieved with flat targets. The structured target optimizes the laser absorption by the electrons. The absorption mechanism is independent of the ion charge in the target, density or thickness, and therefore it is expected to apply for a wide variety of materials.

Our results show that by using nanostructured targets one can obtain energetic ions with a commercially available table-top laser system. This constitutes a robust strategy to produce high energy protons for applications with these table top lasers.

Acknowledgments

This work has been partially supported by the Xunta de Galicia/FEDER under contract Agrup2015/11 (PC034) and by MINECO under contracts MAT2015-71119-R and FIS2015-71933-REDT. The authors would like to acknowledge the OSIRIS Consortium, consisting of UCLA and IST (Lisbon, Portugal) for the use of OSIRIS, for providing access to the OSIRIS framework. M Blanco also thanks the Ministry of Education of the Spanish government for the FPU fellowship. Camilo Ruiz also thanks MINECO project FIS2016-75652-P M Vranic acknowledges the support of ERC-2010-AdG Grant 267841 and LASERLAB-EUROPE IV—GA No. 654148. Simulations were performed at the Accelerates cluster (Lisbon, Portugal).

References

- [1] Macchi A, Borghesi M and Passoni M 2013 *Rev. Mod. Phys.* **85** 751–93
- [2] Daido H, Nishiuchi M and Pirozhkov A S 2012 *Rep. Prog. Phys.* **75** 056401
- [3] Stockem Novo A, Kaluza M C, Fonseca R A and Silva L O 2016 *Sci. Rep.* **6** 29402
- [4] Wilks S C, Langdon A B, Cowan T E, Roth M, Singh M, Hatchett S, Key M H, Pennington D, MacKinnon A and Snavely R A 2001 *Phys. Plasmas* **8** 542–9
- [5] Snavely R A *et al* 2000 *Phys. Rev. Lett.* **85** 2945–8
- [6] Mora P 2003 *Phys. Rev. Lett.* **90** 185002
- [7] Fuchs J *et al* 2005 *Phys. Rev. Lett.* **94** 045004
- [8] MacKinnon A J, Sentoku Y, Patel P K, Price D W, Hatchett S, Key M H, Andersen C, Snavely R and Freeman R R 2002 *Phys. Rev. Lett.* **88** 215006
- [9] Cowan T E *et al* 2004 *Phys. Rev. Lett.* **92** 204801
- [10] Schwoerer H, Pfothner S, Jackel O, Amthor K-U, Liesfeld B, Ziegler W, Sauerbrey R, Ledingham K W D and Esirkepov T 2006 *Nature* **439** 445–8
- [11] Prencipe I *et al* 2016 *Plasma Phys. Control. Fusion* **58** 034019
- [12] Passoni M *et al* 2016 *Phys. Rev. Accel. Beams* **19** 061301
- [13] Sgattoni A *et al* 2013 *Proc. SPIE* **8779** 87790L
- [14] Zheng-Ming S, Su-Ming W, Lu-Le Y, Wei-Min W, Yun-Qian C, Min C and Jie Z 2015 *Chin. Phys. B* **24** 015201
- [15] Bigongiari A, Raynaud M, Riconda C, Hron A and Macchi A 2011 *Phys. Plasmas* **18** 102701

- [16] Raynaud M, Kupersztynch J, Riconda C, Adam J C and Hron A 2007 *Phys. Plasmas* **14** 092702
- [17] Andreev A and Platonov K 2013 *Contrib. Plasma Phys.* **53** 173–8
- [18] Kahaly S, Yadav S K, Wang W M, Sengupta S, Sheng Z M, Das A, Kaw P K and Kumar G R 2008 *Phys. Rev. Lett.* **101** 145001
- [19] Andreev A, Platonov K, Braenzel J, Lübcke A, Das S, Messaoudi H, Grunwald R, Gray C, McGlynn E and Schnrer M 2016 *Plasma Phys. Control. Fusion* **58** 014038
- [20] Margarone D et al 2015 *Phys. Rev. AB* **18** 071304
- [21] Andreev A, Kumar N, Platonov K and Pukhov A 2011 *Phys. Plasmas* **18** 103103
- [22] Klimo O, Psikal J, Limpouch J, Proška J, Novotny F, Ceccotti T, Floquet V and Kawata S 2011 *New J. Phys.* **13** 053028
- [23] Margarone D et al 2012 *Phys. Rev. Lett.* **109** 234801
- [24] Zigler A et al 2013 *Phys. Rev. Lett.* **110** 215004
- [25] Brantov A and Bychenkov V 2013 *Contrib. Plasma Phys.* **53** 731–5
- [26] Dalui M, Wang W-M, Trivikram T M, Sarkar S, Tata S, Jha J, Ayyub P, Sheng Z M and Krishnamurthy M 2015 *Sci. Rep.* **5** 11930
- [27] Andreev A, Platonov K, Braenzel J, Lübcke A, Das S, Messaoudi H, Grunwald R, Gray C, McGlynn E and Schnürer M 2016 *Plasma Phys. Control. Fusion* **58** 014038
- [28] Zigler A et al 2011 *Phys. Rev. Lett.* **106** 134801
- [29] Bigongiari A, Raynaud M, Riconda C and Héron A 2013 *Phys. Plasmas* **20** 052701
- [30] Ceccotti T et al 2013 *Phys. Rev. Lett.* **111** 185001
- [31] Sgattoni A, Fedeli L, Cantono G, Ceccotti T and Macchi A 2016 *Plasma Phys. Control. Fusion* **58** 014004
- [32] Fedeli L et al 2016 *Phys. Rev. Lett.* **116** 015001
- [33] Kupersztynch J, Raynaud M and Riconda C 2004 *Phys. Plasmas* **11** 1669–73
- [34] Riconda C, Raynaud M, Vialis T and Grech M 2015 *Phys. Plasmas* **22** 073103
- [35] Bigongiari A, Raynaud M and Riconda C 2011 *Phys. Rev. E* **84** 015402
- [36] Gibbon P 2005 *Short Pulse Laser Interactions with Matter: An Introduction* (London: Imperial College Press) (<https://doi.org/10.1142/p116>)
- [37] May J, Tonge J, Fiuza F, Fonseca R A, Silva L O, Ren C and Mori W B 2011 *Phys. Rev. E* **84** 025401
- [38] Cialfi L, Fedeli L and Passoni M 2016 *Phys. Rev. E* **94** 053201
- [39] Fonseca R A et al 2002 *Computational Science, ICCS 2002 (Lecture Notes in Computer Science vol 2331)* (Berlin: Springer) pp 342–51
- [40] d’Humières E, Brantov A, Bychenkov V Y and Tikhonchuk V T 2013 *Phys. Plasmas* **20** 023103
- [41] Sgattoni A, Londrillo P, Macchi A and Passoni M 2012 *Phys. Rev. E* **85** 036405